PERGAMON

International Journal of Heat and Mass Transfer 46 (2003) 903–913

International Journal of HEAT and MASS TRANSFER

www.elsevier.com/locate/ijhmt

Temperature effect on single bubble rise characteristics in stagnant distilled water

Tomio Okawa [a,*], Tomoe Tanaka [a], Isao Kataoka [a], Michitsugu Mori [b]

[a] *Department of Mechanophysics Engineering, Osaka University, 2-1, Yamadaoka, Suita-shi, Osaka 565-0871, Japan*
[b] *Nuclear Power R&D Center, Tokyo Electric Power Company, 4-1, Egasaki-cho, Tsurumi-ku, Yokohama-shi, Kanagawa 230-8510, Japan*

Received 12 April 2002

Abstract

Rise characteristics of spherical and ellipsoidal bubbles in normal- and high-temperature distilled water were visually observed. In the high-temperature experiments, the measured results of the rise velocity of a single bubble and the existence of rise path oscillation roughly agreed with the correlations for the bubbles in contaminated liquid. Also, applicability of an available correlation for the frequency of rise path oscillation was confirmed and a new correlation was developed to evaluate the amplitude of oscillation. It is expected that these results are to contribute to the further improvement of the prediction methods of multidimensional void distribution.

1. Introduction

Accurate prediction of critical heat flux in forced-convective flow boiling is often required in the design of industrial plants such as nuclear power reactors. Several mechanisms for the onset of burnout have been proposed [1]; the near wall bubble crowding model by Weisman et al. has shown reasonable success at low and intermediate qualities [2,3]. This suggests that the critical heat flux in bubbly two-phase flow has strong relation with the multidimensional void profile. Thus, one- and multidimensional numerical simulations of bubbly flow have extensively been conducted to accurately predict the void distribution and the critical heat flux in flow boiling [4–7]. Generally, the governing equations used in the bubbly flow simulation consist of the basic equations describing the conservations of mass, momentum and energy and the constitutive equations for mathematical closure. Though the basic equations are derived from the averaging of sufficiently valid local-instantaneous equations [8,9], many constitutive equations have been developed from the experimental data of single bubble rise characteristics in stagnant liquid [10]. Obviously, more complicated phenomena such as turbulence in continuous liquid phase, interaction between bubbles and phase change at the wall should also be taken into account in the case of flow boiling. However, the motion of a single bubble would still be one of the key phenomena to determine the multidimensional void profile; sufficient understanding of the single bubble rise characteristics is considered indispensable to perform accurate numerical simulation of bubbly two-phase flow and consequently to improve the design of nuclear power reactors.

Though numerous studies have been carried out to clarify the rise characteristics of single bubbles [11,12], most experiments have been conducted using normal-temperature liquids and the experimental information on bubble motion in high-temperature liquid is scarce. It is obvious that the bubble motion in high-temperature water is of significant importance from engineering standpoint since high-temperature water is often used as working fluid in various industrial applications. At least, there exist two possible reasons why the bubble motion in high-temperature water could be different from that predicted by available correlations. First, the physical

* Corresponding author. Tel.: +81-6-6879-7257; fax: +81-6-6879-7247.
E-mail address: t-okawa@mech.eng.osaka-u.ac.jp (T. Okawa).

0017-9310/03/$ - see front matter
PII: S0017-9310(02)00345-9

Nomenclature

C_D	drag coefficient
C_R	proportionality factor used in Eq. (7)
d	bubble diameter
Eo	Eötvös number ($= g\rho_l d^2/\sigma$)
g	gravitational acceleration
h	length of minor (vertical) axis of ellipsoidal bubble
Mo	Morton number ($= g\mu_l^4/\rho_l\sigma^3$)
R_A	aspect ratio ($= h/w$)
R_E	eccentricity ($= w/h$)
Re	bubble Reynolds number ($= \rho_l u_b d/\mu_l$)
St	Strouhal number ($= d/u_b t$)
t	period of rise path oscillation
u_b	rise velocity of bubble
u_r	bubble velocity in horizontal direction
We	Weber number ($= \rho_l u_b^2 d/\sigma$)
w	length of major (horizontal) axis of ellipsoidal bubble

Greek symbols

α	amplitude of rise path oscillation
μ	viscosity
ρ	density
σ	surface tension

Subscripts

c	critical
l	liquid

properties such as viscosity and surface tension of high-temperature water are quite different from those of normal-temperature water; the Morton number, that is one of the most important parameters characterizing the bubble motion, is less than the lower limit of most experimental databases. Thus, the available correlations might not be applicable to the bubbles in such a low Morton number fluid. Second, the vapor pressure rapidly increases as the fluid temperature approaches to the saturation temperature. Hence, the phase change at the bubble interface should become prominent in high-temperature liquid; it is probable that the interface condition and consequently the bubble motion are affected by the increased phase change rate at the interface. In fact, Fan and Tsuchiya pointed out that their correlation for the terminal bubble rise velocity is reasonably accurate in wide range of experimental conditions and one exception is the bubbles in hot tap water [12]. It could hence be said that more experimental data are still needed to sufficiently understand the bubble motion in high-temperature water.

In view of these, rise characteristics of spherical and ellipsoidal bubbles in normal- and high-temperature distilled water are visually observed in the present study. All the experiments are conducted under the atmospheric pressure. It is however noted that the Morton number in the present high-temperature experiments is about 5×10^{-13}; this value is of the same order with that of the saturated water at higher pressure ($Mo \approx 2 \times 10^{-13}$ at 7 MPa, for example). Also, the vapor pressure is not negligible in high-temperature experiments since the water temperature is near the saturation temperature. It is hence expected that the results of the present high-temperature experiments could be applicable not only to the bubble motion in the atmospheric pressure but also to that in the higher temperature water at elevated pressure. Since the bubble motion could depend on the initial distortion at the detachment from an injection nozzle or heated surface, several methods are tested for bubble formation. In the numerical simulations of bubbly two-phase flow, the bubble rise velocity relative to the local liquid velocity and the rise path oscillation are important parameters [7]. First, the relative velocity affects the lateral force acting on a bubble as well as the bubble rise velocity itself. Hence, the lateral void distribution and the cross-sectional area-averaged void fraction significantly depend upon the relative velocity. Next, the rise path oscillation such as zigzag and spiral motions is related to the spatial development of void profile. Also, it is known that the bubble rise velocity and the rise path oscillation have the strong relation with the bubble shape [11,12]. For this reason, the present observation is focused on the shape, rise velocity and oscillatory motion of single bubbles. In the followings, the experimental setup and measurement methods are described. Then, the results and several recommended correlations are shown.

2. Description of the experiments

2.1. Experimental setup

The experimental setup is shown schematically in Fig. 1. The size of the rectangular transparent vessel is 250 mm in width, 300 mm in depth and 400 mm in height. Five K-type thermocouples, two heaters and three bubble injection tubes are equipped in the vessel. In the experiments, the test vessel is filled with distilled water; then, two heaters are used to increase the water temperature. To reveal the temperature effect on bubble motion, the experiments are conducted in normal and

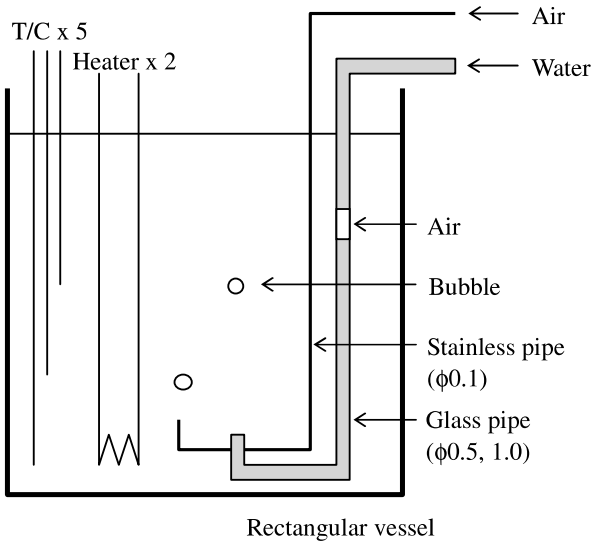

Fig. 1. Schematic diagram of test facility.

high temperatures. After the water temperature reaches a prescribed value, air bubbles are injected from one of the three tubes or vapor bubbles are generated by the heater to record the rise characteristics of bubbles.

The thermocouples were equipped at various distances from the wall and elevations, but the maximum difference between the five temperatures was less than 1.0 °C. Hence, the water temperature in the vessel was considered sufficiently uniform in each experiment. It is known that the bubble motion significantly depends on the liquid purity [11,12], but it was recently reported that the bubble motion also depends on the initial distortion at the detachment and the bubble behavior in pure liquid can be similar to that in impure liquid if the initial distortion is sufficiently small [13]. Hence, to examine the effect of initial distortion at the detachment, the three bubble injection tubes summarized in Table 1 are used in the present experiments. The first and second tubes are made of Pyrex glass and their inner diameters are 1.0 and 0.5 mm, respectively. When a glass tube is used to inject air bubbles, the tube is filled with distilled water and small amount of air is inserted from the micro-syringe into the tube (see Fig. 1); further injecting water from the end of the tube, the air is pushed into the test vessel that results in a single bubble. This method of bubble injection is named controlled injection in the present study. The third injection tube is a stainless steel pipe whose inner diameter is 0.1 mm. When this injection tube is used, air was directly injected from the end of the pipe; this method is named direct injection. In this case, some amount of air is torn off at the other end of the pipe; this usually creates several bubbles. There is one more method to generate bubbles. In this case, vapor bubbles are created by one of the heaters that are primarily used to increase the water temperature. When the nozzle diameter is smaller than the bubble size, the bubble should deform at the detachment. Furthermore, air is torn off at the detachment in the direct injection. Hence, significant initial distortion is probable to be induced when bubbles are directly injected from the

Table 1
Methods of bubble formation

Source of bubbles	Method of bubble formation	Expected distortion at the detachment	Temperature (°C)	
			Normal[a]	High[a]
Glass pipe (∅1.0)	Controlled injection	Small	13.6 (12) 17.8 (11)	86.7 (13)
Glass pipe (∅0.5)	Controlled injection	Medium	12.7 (9) 14.7 (16)	89.5 (25)
Stainless pipe (∅0.1)	Direct injection	Large	14.3 (10) 13.2 (8)	90.5 (8)
Heater	Boiling	Unknown	–	99.3 (20)

[a] The number of data in each temperature is shown in parenthesis.

stainless steel pipe. While, the initial distortion would be smallest when the glass pipe of 1.0 mm in diameter is used and intermediate when the glass pipe of 0.5 mm is used. The initial distortion induced to vapor bubbles at the detachment from heated surface is not clear, so that it is investigated from the bubble rise characteristics after the detachment.

In the case of air bubbles, the experiments are conducted in normal temperatures about 15 °C and in high temperatures about 90 °C to reveal the temperature effect on bubble motion. While, in the case of vapor bubbles, the liquid should be almost saturated. The temperature and the number of data in each experiment are also summarized in Table 1.

2.2. Measurement method

To measure the sizes, shapes, rise velocities and rise paths of bubbles, the stereo-images of rising bubbles are obtained by carefully positioned two high-speed video cameras. The elevation of the cameras is approximately 200 mm above the bubble injection point. From existing experimental data [14], the detachment of a bubble from an injection nozzle can result in its strong deformation that is followed by a series of shape oscillation, but it rapidly decays after a few cycles by the bridling effects of viscous forces and surface tension. It is hence considered in the present experiments that the bubble motion is measured after the bubble rises up sufficiently long distance. The video images are captured every 4 ms with the shutter speed of 1 ms; the frame resolution adopted is 1024×1024 (approximately 12×12 pixels are included in the square region of 1 mm^2). Though single bubbles are to be created in the controlled injection, multiple bubbles are created at the same time in the direct injection and boiling. Since the leading bubbles often affect the behavior of trailing ones when multiple bubbles exist [15,16], the data for the trailing bubbles are not used to avoid the effects of other bubbles.

Since the pixel size of video image is less than 0.1 mm, the positions and velocities of bubbles are to be measured with reasonable accuracy; the estimated measurement errors of bubble position and rise velocity are less than ± 0.1 mm and ± 2 mm/s, respectively. However, in the measurement of bubble size, some difficulty arises from the bubble distortion. When the bubble is sufficiently small, bubble size is accurately to be measured since the bubble is almost spherical shape. However, when the bubble size is larger, the bubble shape is changed from spherical to ellipsoidal. To evaluate the size of ellipsoidal bubble, we assumed that the bubble has ideal ellipsoidal shape whose minor (vertical) axis is the axis of symmetry. In the evaluation of the sphere-equivalent diameter d of an ellipsoidal object, the lengths of minor axis h and major axis w are needed. To accurately measure these two lengths, the bubble should be observed along its major axis. Thus, further assuming that the bubble moves in the direction of its minor axis [12], the two lengths are measured when the bubble rise path is expected to be parallel to the lens of camera. Under the above assumptions, this condition is satisfied at the following instant: (1) If the rise path is straight, the rise path is always parallel to the lens. (2) If the rise path is zigzag, it becomes parallel at the top of oscillation. (3) If the rise path is spiral, it becomes parallel at the center of two successive tops of oscillatory motion captured in the video image. The size of each bubble was measured twice using the two video images captured by the camera A and camera B; the two measured sizes of air bubbles are compared in Fig. 2. If the present assumptions are correct, the bubble size measured from the image by the camera A should agree with that by the camera B. As indicated in Fig. 2, most data agree with each other within the error of 10%. The above assumptions on the bubble shape are hence expected to be reasonably right and the measurement error in the bubble size is estimated to be less than 10% in the case of air bubbles.

It should however be noted that the accuracy of measurement is deteriorated in the experiments of vapor bubbles. In this case, a number of bubbles were created at the same time and the correspondence between the two bubble images captured by cameras A and B was not to be taken. Thus, the rise characteristics of vapor bubbles were evaluated from the video image by one camera. Also, in this case, natural circulation formed in the vessel might not be negligible comparing with the bubble rise velocity,

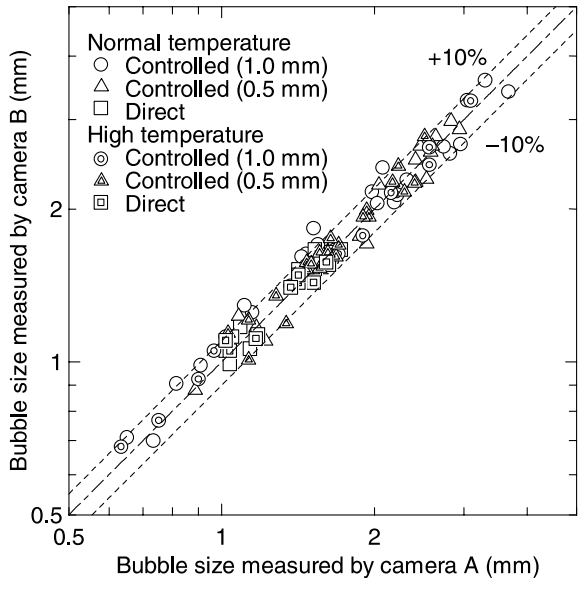

Fig. 2. Comparisons of bubble sizes measured by two cameras.

so that the measured rise velocities of vapor bubbles should be slightly higher than the true rise velocity in stagnant medium. Hence, in the following chapter, the results for air bubbles are primarily shown and the results for vapor bubbles are additionally described.

3. Results and discussion

3.1. Bubble shape

The bubbles in the present experiments were spherical or ellipsoidal, so that the bubble shape is characterized by the aspect ratio R_A. Since the buoyancy and surface tension are important parameters in the determination of bubble shape, R_A is plotted against the Eötvös number Eo in Fig. 3. As indicated in the figure, R_A monotonously decreases with Eo, but the dependence on the method of bubble formation is clearly seen. This implies that the bubble shape is significantly affected by the condition at the detachment. The aspect ratio becomes smaller when the initial distortion is more prominent. The upper boundary of R_A is roughly given by the following correlation by Wellek et al. for contaminated systems [17]:

$$R_A = \frac{1}{1 + 0.163 Eo^{0.757}} \tag{1}$$

Paying the attention to the data for the bubbles from the largest-diameter tube, it is found that the above correlation provides reasonable predictions for smaller bubbles but it over-estimates the aspect ratio for larger bubbles. Since the tube diameter is 1.0 mm and the range of bubble size is 0.6–3.5 mm, larger bubbles would suffer notable distortion at the detachment even if the largest-diameter tube is used. It is hence considered that the bubble shape in clean water is significantly affected by the method of bubble formation but the shape is similar to that in contaminated liquid if the initial distortion at the detachment is sufficiently small. While, within the present experimental conditions ($Eo < 1$), the following correlating line is recommended for the lower boundary:

$$R_A = \frac{1}{1 + 1.97 Eo^{1.3}} \tag{2}$$

The measured aspect ratio is next compared with the correlation by Moore [18] in Fig. 4. This correlation is derived from the theoretical investigation of the force acting on an ellipsoidal bubble and given by

$$We = \frac{4(R_E^3 + R_E - 2)\left[R_E^2 \sec^{-1} R_E - (R_E^2 - 1)^{1/2}\right]^2}{R_E^{4/3}(R_E^2 - 1)^3} \tag{3}$$

where R_E is the eccentricity defined as the inverse of aspect ratio. Though significant scattering still remains, Fig. 4 shows that the aspect ratio is roughly correlated as a function of the Weber number. This implies that inertia and surface tension play an important role in determining the bubble shape.

3.2. Rise velocity

The bubble rise velocity u_b in still liquid is an important parameter in the numerical simulation of bubbly

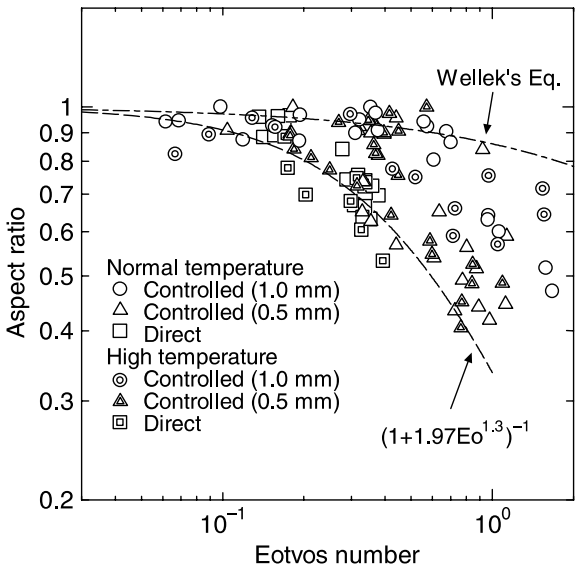

Fig. 3. Aspect ratio of bubble shape as a function of Eötvös number.

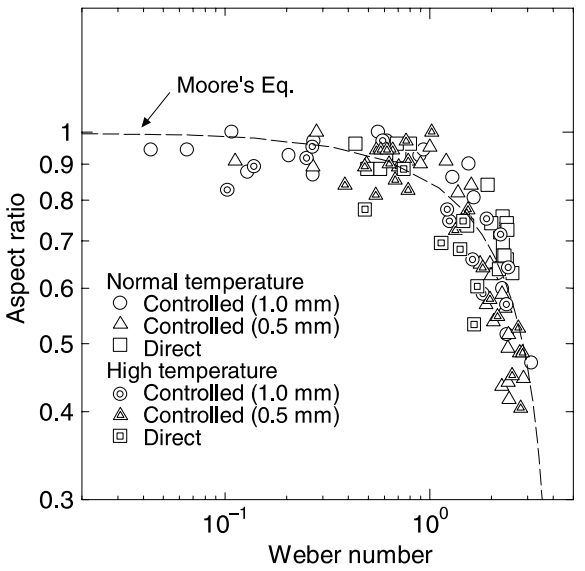

Fig. 4. Comparison of measured aspect ratio with the correlation of Moore.

two-phase flow since it is often used as the basis of the correlation for the drag coefficient. First, the measured bubble rise velocities in normal-temperature water are compared with several correlations for pure liquid and impure liquid in Fig. 5(a) and (b), respectively [10,12,19]; the details of these correlations are given in Appendix A. These figures reveal that the rise velocities of bubbles generated by direct injection agree with the correlations for pure liquid and the bubble rise velocities for controlled injection from the largest-diameter tube correspond to those for impure liquid; the rise velocities for 0.5 mm diameter pipe are intermediate. It is hence confirmed that the bubble rise velocity depends on the initial distortion as well as liquid purity, which agrees with the observation by Tomiyama et al. [13].

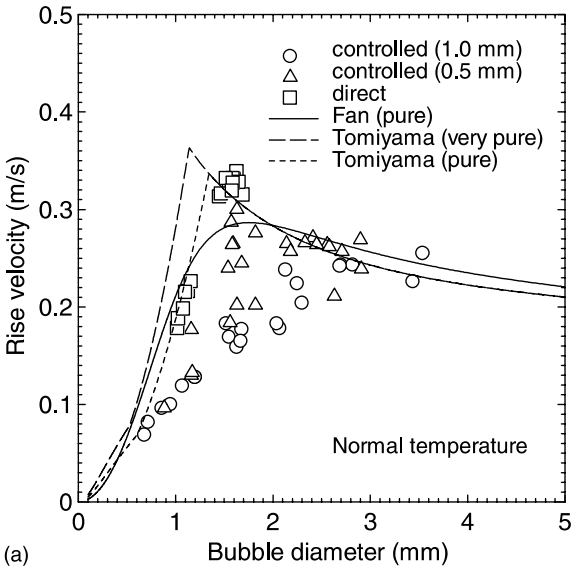

(a)

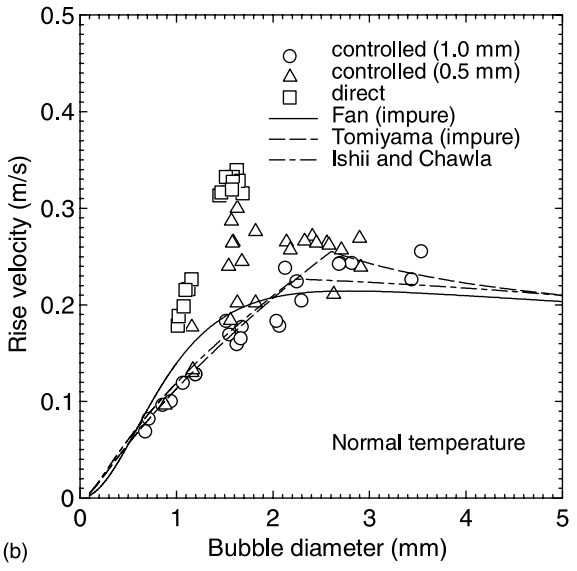

(b)

Fig. 5. Bubble rise velocity in normal-temperature water: (a) comparisons with the correlations for bubbles in pure liquid, (b) comparisons with the correlations for bubbles in impure liquid.

The measured rise velocities of air bubbles in high-temperature water are compared with the same correlations in Fig. 6(a) and (b). Though the rise velocity is higher when the initial distortion is largest, the effect of the method of bubble formation is markedly reduced. In particular, the high rise velocity corresponding to the correlation for pure liquid is not measured and the rise velocities for all the three bubble injection methods roughly agree with the correlations for impure liquid. Hence, as the first approximation, the use of the correlation for impure liquid is recommended from the present experimental data to estimate the bubble rise velocity in high-temperature water. The primary reason for the slower rise velocity in high-temperature water is not clear, but the possible mechanism is described as follows. When the fluid temperature is near the saturation temperature, the phase change rate would not be negligible due to the increased vapor pressure. It is hence probable that the phase change through phase interface affects the interfacial condition and consequently the rise velocity. In the correlation of Fan and Tsuchiya [12], the parameter n is used to account the liquid purity. The standard value of n is 1.6 and 0.8 for clean and contaminated liquids, respectively, but a smaller value is recommended for hot tap water. As indicated in Fig. 6(c), the values of 1.35 and 0.55 approximate the upper and lower boundaries of measured rise velocities in the present experiments.

3.3. Rise path oscillation

When the bubble size is sufficiently small, the bubble rise path is almost rectilinear; while, as the bubble size increases, the rise path oscillation is triggered and the rise path becomes zigzag or spiral. Since the diffusive property of void distribution in bubbly two-phase flow depends on the oscillatory bubble motion [7,20], the rise path oscillation is investigated. From the existing knowledge [21], the onset of oscillation takes place at the constant bubble Reynolds number in contaminated liquid:

$$Re_c = 202 \tag{4}$$

While, in clean liquid, the critical Reynolds number is expressed in terms of the Morton number:

$$Re_c = 9.0Mo^{0.173} \tag{5}$$

According to these correlations, the rise path oscillation is more easily induced in contaminated liquid. The onset of rise path oscillation is compared with these correlations in Fig. 7(a)–(c). In normal-temperature water

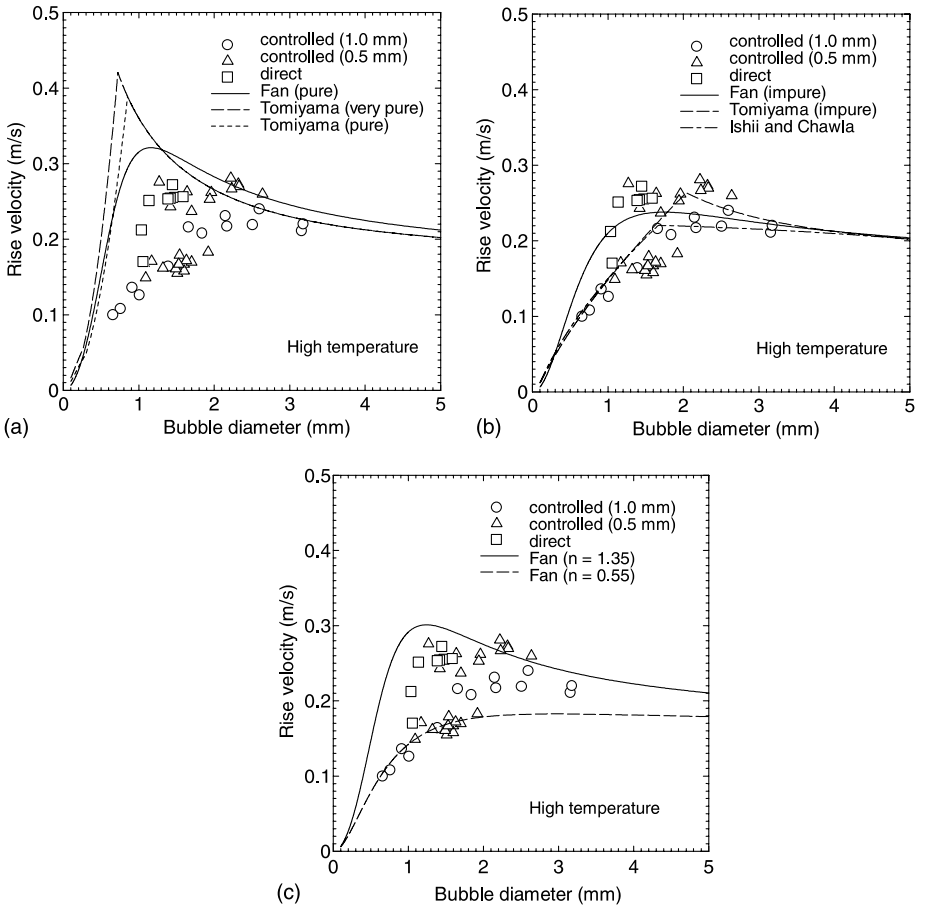

Fig. 6. Bubble rise velocity in high-temperature water: (a) comparisons with the correlations for bubbles in pure liquid, (b) comparisons with the correlations for bubbles in impure liquid, (c) recommended values for the parameter n in the correlation of Fan and Tsuchiya.

($Mo \approx 3 \times 10^{-11}$), the condition for the onset of oscillation is roughly approximated by the correlation for clean liquid when the bubbles are directly injected and it agrees with the correlation for contaminated liquid in other injection methods. While, in high-temperature water ($Mo \approx 5 \times 10^{-13}$), it was difficult to create a small-diameter bubble whose Reynolds number is less than 202 due to reduced viscosity. Thus, the critical Reynolds number is not determined from the measured data. However, the oscillatory motion is observed under the critical bubble Reynolds number evaluated by Eq. (5). Also, when a bubble is injected from the largest-diameter nozzle, the boundary agrees with the prediction by Eq. (4). It is hence expected in the high-temperature water that the onset of rise path oscillation is approximated by the correlation for contaminated liquid (Eq. (4)). These results of the onset of rise path oscillation correspond to the measured results of rise velocity shown in Figs. 5 and 6. Namely, an appropriate correlation for the bubble motion in normal-temperature water depends on the injection method; while, the bubble motion in high-temperature water is roughly predicted by the correlation for contaminated liquids.

The frequency and amplitude of rise path oscillation are investigated. First, the Strouhal number St is compared with the following Tsuge's correlation [22] in Fig. 8:

$$St = 0.1 C_D^{0.734} \tag{6}$$

As shown in the figure, the present experimental data agree with the above correlation within the error of $\pm 30\%$. This implies that the oscillation frequency is roughly to be predicted if the size and rise velocity of a bubble are given. Next, a new correlation for the amplitude of rise path oscillation is developed since widely accepted correlation is not available in literature. If the bubble velocity in the horizontal direction u_r is proportional to its vertical component u_b, the dimensionless

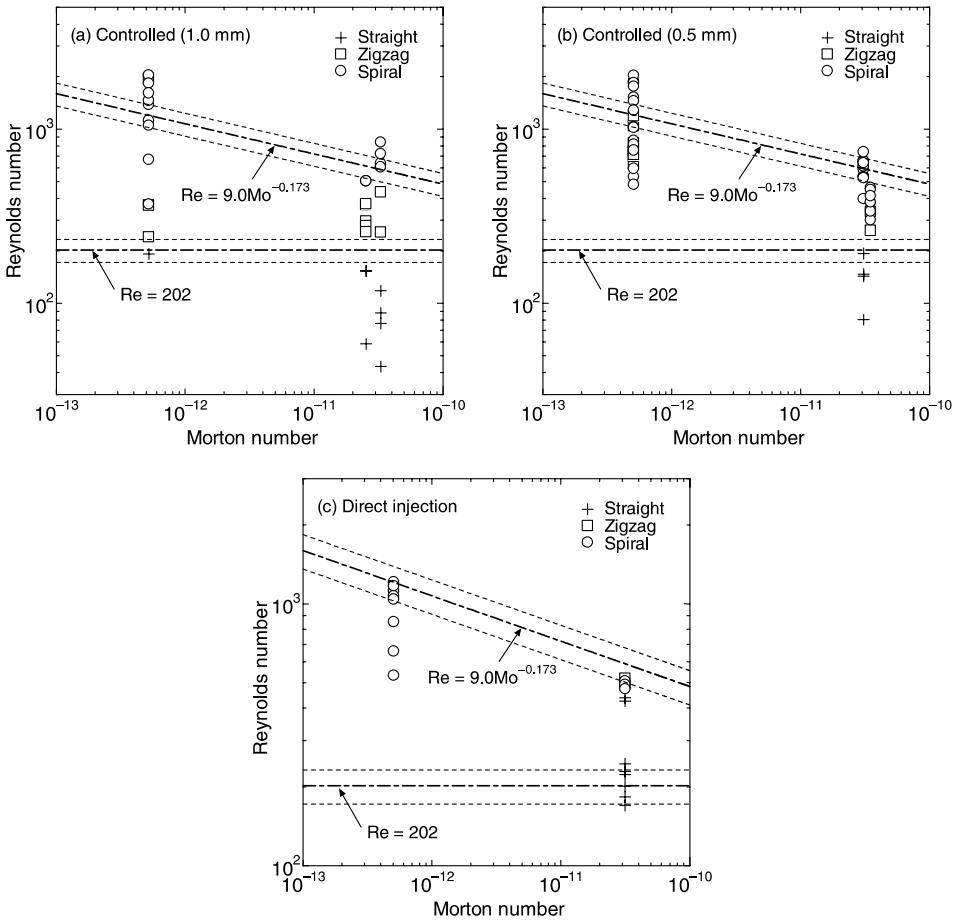

Fig. 7. Bubble rise path in each experimental condition: (a) controlled injection from 1.0 mm tube, (b) controlled injection from 0.5 mm tube, (c) direct injection.

amplitude of the oscillatory motion α/d should be inversely proportional to St. For this reason, α/d is plotted against St in Fig. 9(a). As shown in the figure, most data of α/d are proportional to St^{-1}; however, the amplitude is significantly smaller in some experimental conditions. If the results shown in Fig. 9(a) are carefully investigated, it is found that the dimensionless amplitude is small when the bubble Reynolds number is near the critical value for the onset of oscillation Re_c. It is hence expected that α/d is to be correlated by

$$\frac{\alpha}{d} = C_R St^{-1} \tag{7}$$

where the coefficient C_R is given as a function of Re. The relation between $Re - Re_c$ and C_R is shown in Fig. 9(b) where Re_c is set at 450 from experimental data in the direct injection at the normal temperature and estimated by Eq. (4) in other experimental conditions. Though scattering still exists, the general trend is captured by

$$C_R = 0.1 \times \left\{1 - e^{-0.0061(Re - Re_c)}\right\} \tag{8}$$

Substituting the above equation to Eq. (7), the amplitude of rise path oscillation is evaluated.

3.4. Rise characteristics of vapor bubbles

The bubble number density could not be kept sufficiently low when vapor bubbles were created by the heater. Consequently, weak natural circulation was formed in the vessel; also, the bubble image corresponding to the bubble captured by the other camera could not be distinguished. It should hence be noted that the measured bubble rise characteristics contain larger errors in this case. However, qualitative examination would still be possible. The measured rise velocities of vapor bubbles are compared with the correlations for contaminated system in Fig. 10. Since there existed multiple bubbles in the experiment, the bubbles not strongly affected by the leading ones were selected to

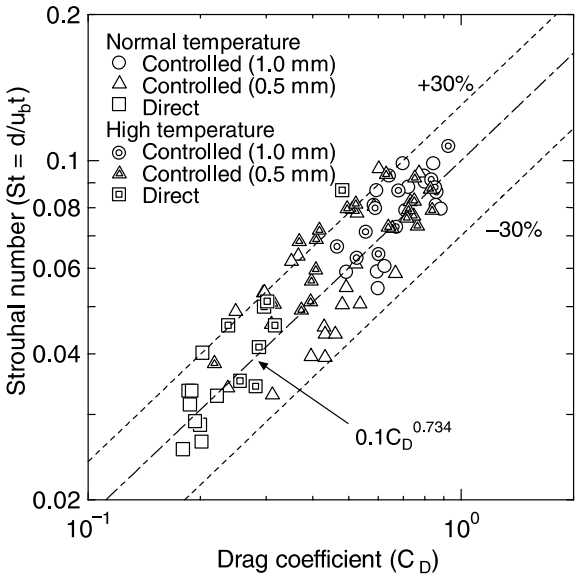

Fig. 8. Relation between drag coefficient and Strouhal number.

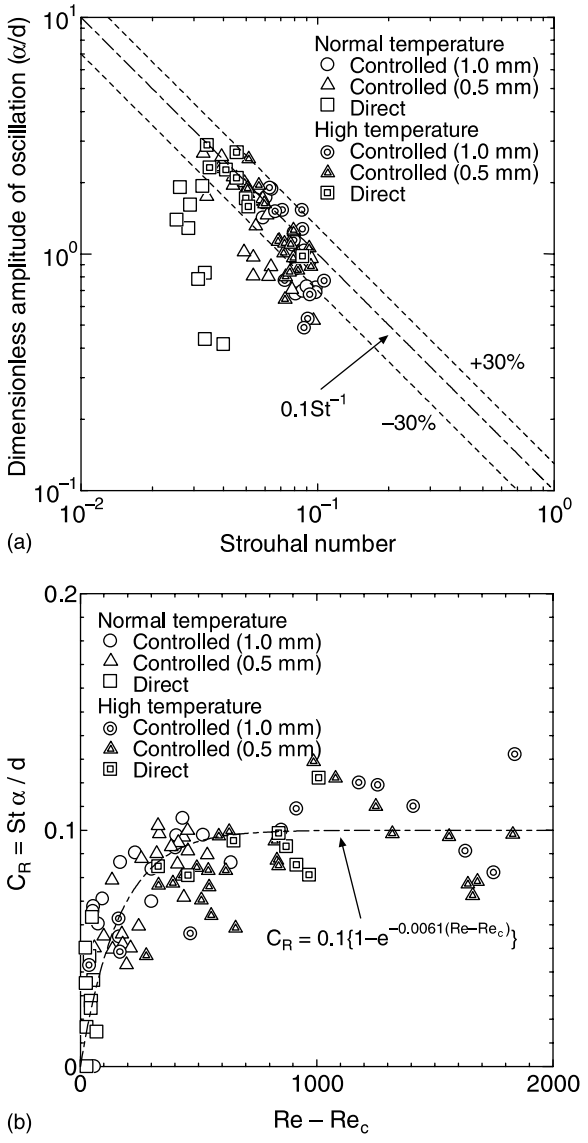

Fig. 9. Correlation for the amplitude of rise path oscillation: (a) relation between Strouhal number and dimensionless amplitude, (b) dependence of coefficient C_R on bubble Reynolds number.

derive the rise velocity. As shown in Fig. 10, the rise velocities of vapor bubbles reasonably agree with the correlations for contaminated system. Though the correlations slightly under-predict the present experimental data, it would primarily be because the bubble rise velocity was increased by the natural circulation flow. Next, the existence of rise path oscillation is plotted in *Mo–Re* map in Fig. 11. Since all the measured bubbles exhibited oscillatory motion, the lower boundary of oscillation is not determined from the present data. However, since the oscillatory motion is observed below the condition estimated by Eq. (5), the correlation for the contaminated system Eq. (4) would be appropriate for vapor bubbles. These results of the rise velocity and the onset of rise path oscillation of a vapor bubble agree with those for air bubbles in high-temperature water. It is hence expected that the initial distortion at the detachment from heating surface is not prominent to alter the rise characteristics and the correlations for the air bubbles in high-temperature water are applicable to describe the rise characteristics of vapor bubbles.

4. Summary and conclusions

Bubble behavior in high-temperature water is of significant importance in many industrial applications; however, most experiments on bubble motion have been conducted in normal-temperature liquid. In view of this, single bubble rise characteristics in distilled water were experimentally investigated in high- as well as normal-temperature conditions. Since the bubble rise characteristics could depend on initial distortion, several methods were tested for the formation of bubbles. Using the two high-speed video cameras, the sizes, shapes, rise velocities and rise paths of single bubbles were precisely measured. The range of sphere-equivalent bubble diameter was 0.6–3.7 mm; the bubble shape was spherical or ellipsoidal. The main conclusions derived from the present experimental observations are summarized as follows:

(1) In normal-temperature water, the rise velocity and the condition for the onset of rise path oscillation are affected by the method of bubble formation.

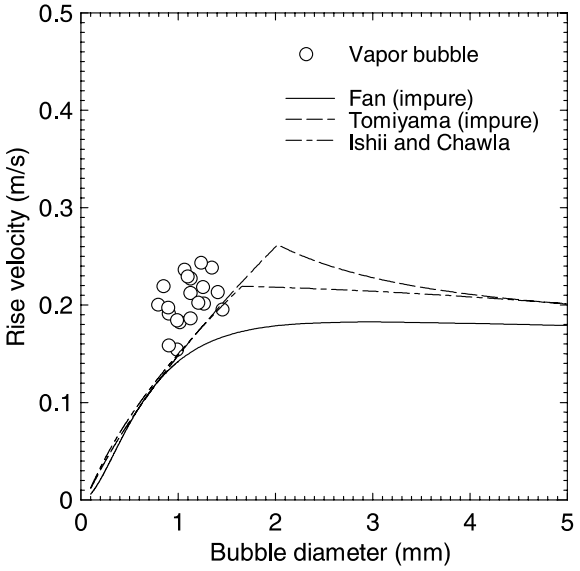

Fig. 10. Rise velocities of vapor bubbles in saturated water.

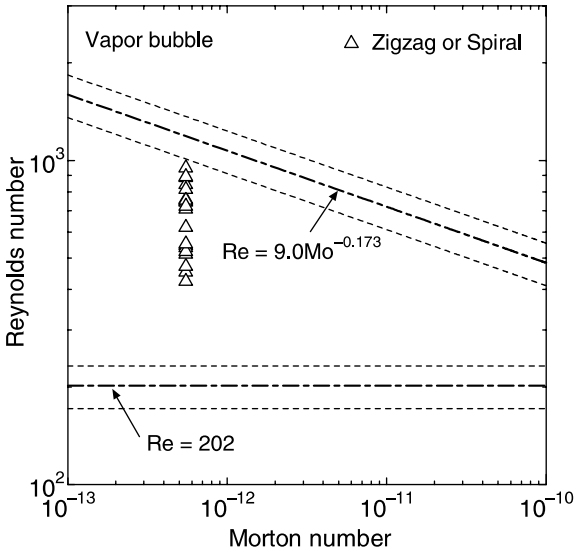

Fig. 11. Existence of rise path oscillation for vapor bubbles in saturated water.

The available correlations for pure liquids are appropriate when the initial distortion is sufficient, but those for contaminated liquids are preferable even in distilled water if the initial distortion is small.

(2) The dependence of bubble rise velocity on the injection method was observed even in high-temperature water. In the present experiments, however, all the rise velocities were roughly predicted by the correlations for contaminated liquids and the correlation for pure liquids was not applicable to the onset of rise path oscillation. The same results were also obtained in the case of vapor bubbles created by heater. It could hence be said that the effects of initial distortion are reduced and the correlations for contaminated liquids are recommended as the first approximation for the bubble motion in high-temperature water.

(3) The frequency of rise path oscillation is satisfactorily correlated in terms of drag coefficient in high-temperature as well as normal-temperature conditions. If the bubble Reynolds number is sufficiently larger than the critical value for the onset of oscillation, the lateral component of bubble velocity is almost proportional to the vertical component and the amplitude of oscillation is correlated in terms of the Strouhal number. When the bubble Reynolds number is near the critical value, the lateral component and consequently the amplitude of oscillation are reduced; a new correlation was proposed to accurately predict the amplitude of rise path oscillation in whole range of Reynolds number above the critical value.

(4) The bubble shape is significantly affected by the injection method. The maximum aspect ratio is observed when the initial distortion is small and it is approximated by the correlation by Wellek for contaminated systems. The increase of initial distortion results in the smaller aspect ratio and the faster rise velocity. It was found that the lower boundary of aspect ratio is correlated in terms of the Eötvös number and the relation between the bubble shape and bubble rise velocity is roughly described by Moore's theory.

Appendix A. Correlations for terminal bubble rise velocity

The three correlations for terminal bubble rise velocity used in the present study are described. In the correlation by Fan and Tsuchiya [12], the rise velocity is correlated by

$$u_{\mathrm{b}} = \left(u_{\mathrm{b1}}^{-n} + u_{\mathrm{b2}}^{-n}\right)^{-1/n} \tag{A.1}$$

where

$$u_{\mathrm{b1}} = \frac{\rho_{\mathrm{l}} g d^2}{K_{\mathrm{b}} \mu_{\mathrm{l}}} \tag{A.2}$$

$$u_{\mathrm{b2}} = \sqrt{\frac{2c\sigma}{\rho_{\mathrm{l}} d} + \frac{gd}{2}} \tag{A.3}$$

The three parameters K_{b}, c and n are included in these equations. If the liquid is water, K_{b} is given by

$$K_{\mathrm{b}} = \max[12, 14.7Mo^{-0.038}] \tag{A.4}$$

The value of c is 1.2 for mono-component liquids; the standard value of n is 1.6 and 0.8 for clean and contaminated systems, respectively, but a smaller value is suggested for hot tap water.

The other two correlations are for the drag coefficient. Using the drag coefficient C_D, the bubble rise velocity is expressed by

$$u_b = \sqrt{\frac{4gd}{3C_D}} \tag{A.5}$$

The three correlations have been proposed by Tomiyama for different contamination levels [19]:

$$C_D = \max\left[\min\left\{\frac{16}{Re}(1+0.15Re^{0.687}), \frac{48}{Re}\right\}, \frac{8}{3}\frac{Eo}{Eo+4}\right]$$
for clean liquid (A.6)

$$C_D = \max\left[\min\left\{\frac{24}{Re}(1+0.15Re^{0.687}), \frac{72}{Re}\right\}, \frac{8}{3}\frac{Eo}{Eo+4}\right]$$
for slightly contaminated liquid (A.7)

$$C_D = \max\left[\frac{24}{Re}(1+0.15Re^{0.687}), \frac{8}{3}\frac{Eo}{Eo+4}\right]$$
for fully contaminated liquid (A.8)

The correlation by Ishii and Chawla is for contaminated liquids and given by [10]

$$C_D = \max\left[\frac{24}{Re}(1+0.1Re^{0.75}), \min\left\{\frac{2}{3}\sqrt{\frac{\rho_l g d^2}{\sigma}}, \frac{8}{3}\right\}\right] \tag{A.9}$$

References

[1] G.F. Hewitt, Burnout, in: G. Hetsroni (Ed.), Handbook of Multiphase Systems, McGraw-Hill, New York, 1982, pp. 6.66–6.141.

[2] J. Weisman, B.S. Pei, Prediction of critical heat flux in flow boiling at low qualities, Int. J. Heat Mass Transfer 26 (10) (1983) 1463–1477.

[3] S.H. Ying, J. Weisman, Prediction of the critical heat flux in flow boiling at intermediate qualities, Int. J. Heat Mass Transfer 29 (11) (1986) 1639–1648.

[4] N. Kurul, M.Z. Podowski, Multidimensional effects in forced convective subcooled boiling, in: Proceeding of the Ninth International Heat Transfer Conference, Jerusalem, 1990, pp. 21–26.

[5] J.C. Lai, B. Farouk, Numerical simulation of subcooled boiling and heat transfer in vertical ducts, Int. J. Heat Mass Transfer 36 (6) (1993) 1541–1551.

[6] I. Kataoka, S. Kodama, A. Tomiyama, A. Serizawa, Study on analytical prediction of forced convective CHF based on multi-fluid model, Nucl. Eng. Design 175 (1997) 107–117.

[7] T. Okawa, I. Kataoka, M. Mori, Numerical simulation of lateral phase distribution in turbulent upward bubbly two-phase flows, Nucl. Eng. Des. 213 (2002) 183–197.

[8] M. Ishii, Thermo-Fluid Dynamic Theory of Two-Phase Flow, Eyrolles, Paris, 1975.

[9] D.A. Drew, Analytical modeling of multiphase flows, in: R.T. Lahey (Ed.), Boiling Heat Transfer, Elsevier, Amsterdam, 1992, pp. 31–84.

[10] M. Ishii, T.C. Chawla, Local drag laws in dispersed two-phase flow, NUREG/CR-1230, ANL-79-105, 1979.

[11] R. Clift, J.R. Grace, M.E. Weber, Bubbles, Drops, and Particles, Academic Press, New York, 1978.

[12] L.-S. Fan, K. Tsuchiya, Bubble Wake Dynamics in Liquids and Liquid-Solid Suspensions, Butterworth-Heinemann, Oxford, 1990.

[13] A. Tomiyama, S. Yoshida, S. Hosokawa, Surface tension force dominant regime of single bubbles rising through stagnant liquids, in: Proceedings of the UK-Japan Seminar on Multiphase Flow, Bury St Edmunds, 2001.

[14] H. Kalman, A. Ullmann, Experimental analysis of bubble shapes during condensation in miscible and immiscible liquids, Trans. ASME, J. Fluids Eng. 121 (1999) 496–502.

[15] J.R. Crabtree, J. Bridgwater, Bubble coalescence in viscous liquids, Chem. Eng. Sci. 26 (1971) 839–851.

[16] T. Okawa, K. Yoneda, Y. Yoshioka, New interfacial drag force model including effect of bubble wake (I); Model development for steam-water bubbly flow in large-diameter pipe, J. Nucl. Sci. Technol. 35 (12) (1998) 895–904.

[17] R.M. Wellek, A.K. Agrawal, A.H.P. Skelland, Shape of liquid drops moving in liquid media, AIChE J. 12 (1966) 854–862.

[18] D.W. Moore, The rise of a gas bubble in a viscous liquid, J. Fluid Mech. 6 (1959) 113–130.

[19] A. Tomiyama, Struggle with computational bubble dynamics, in: Proceedings of the third International Conference on Multiphase Flow, Lyon, Paper No. 004, 1998.

[20] T. Okawa, K. Araki, K. Yoshida, T. Matsumoto, I. Kataoka, M. Mori, Numerical simulation of single bubbles located in turbulent flow in vertical pipes using bubble tracking method, Jpn. J. Multiphase Flow 15 (2) (2001) 165–174.

[21] H. Tsuge, S. Hibino, J. Chem. Eng. Jpn. 10 (1977) 66.

[22] H. Tsuge, S. Hibino, The motion of single gas bubbles rising in various liquids, Kagaku Kogaku 35 (1) (1971) 65–70 (in Japanese).